

Beyond Multilayer Perceptrons: Investigating Complex Topologies in Neural Networks

Tommaso Boccato¹, Matteo Ferrante¹, Andrea Duggento^{1,#}, Nicola Toschi^{1,2,#}

{tommaso.boccato,matteo.ferrante}@uniroma2.it

{duggento,toschi}@med.uniroma2.it

¹Department of Biomedicine and Prevention, University of Rome Tor Vergata, Rome, Italy

²A.A. Martinos Center for Biomedical Imaging and Harvard Medical School, Boston, USA

#These authors contributed equally to this work

Abstract

In this study, we explore the impact of network topology on the approximation capabilities of artificial neural networks (ANNs), with a particular focus on complex topologies. We propose a novel methodology for constructing complex ANNs based on various topologies, including Barabási-Albert, Erdős-Rényi, Watts-Strogatz, and multilayer perceptrons (MLPs). The constructed networks are evaluated on synthetic datasets generated from manifold learning generators, with varying levels of task difficulty and noise.

Our findings reveal that complex topologies lead to superior performance in high-difficulty regimes compared to traditional MLPs. This performance advantage is attributed to the ability of complex networks to exploit the compositionality of the underlying target function. However, this benefit comes at the cost of increased forward-pass computation time and reduced robustness to graph damage.

Additionally, we investigate the relationship between various topological attributes and model performance. Our analysis shows that no single attribute can account for the observed performance differences, suggesting that the influence of network topology on approximation capabilities may be more intricate than a simple correlation with individual topological attributes.

Our study sheds light on the potential of complex topologies for enhancing the performance of ANNs and provides a foundation for future research exploring the interplay between multiple topological attributes and their impact on model performance.

1 Introduction

Modern neural architectures are widely believed to draw significant design inspiration from biological neuronal networks. The artificial neuron, the fundamental

functional unit of neural networks (NNs), is based on the McCulloch-Pitts unit [13], sharing conceptual similarities with its biological counterpart. Additionally, state-of-the-art convolutional NNs incorporate several operations directly inspired by the mammalian primary visual cortex, such as nonlinear transduction, divisive normalization, and maximum-based pooling of inputs. However, these architectures may be among the few examples where the evolutionary structural and functional properties of neuronal systems have been genuinely relevant for NN design. Indeed, the topology of biological connectomes has not yet been translated into deep learning model engineering.

Due to the ease of implementation and deployment, widely-used neural architectures predominantly feature a regular structure resembling a sequence of functional blocks (e.g., neuronal layers). The underlying multipartite graph of a multilayer perceptron (MLP) is typically controlled by a few hyperparameters that define its basic topological properties: depth, width, and layer sizes. Only recently have computer vision engineers transitioned from chain-like structures [32] to more elaborate connectivity patterns [16, 17] (e.g., skip connections, complete graphs). Nevertheless, biological neuronal networks display much richer and less templated wirings at both the micro- and macro-scale [14]. Considering synaptic connections between individual neurons, the *C. elegans* nematode features a hierarchical modular [5] connectome, wherein hubs with high betweenness centrality are efficiently interconnected [4, 33]. Moreover, the strength distribution of the adult *Drosophila* central brain closely follows a power law with an exponential cutoff [29].

As a result, the relationship between the graph structure of a NN and its predictive abilities remains unclear. In the literature, there is evidence that complex networks can be advantageous in terms of predictive accuracy and parameter efficiency [18]. However, past attempts to investigate this connection have yielded conflicting results that are difficult to generalize outside the investigated context. The first experiment on complex NNs was performed in 2005 by Simard et al., who trained a randomly rewired MLP on random binary patterns [31]. Nearly a decade later, ErKaymaz and his collaborators employed the same experimental setup on various real-life problems [12, 11, 9, 10] (e.g., diabetes diagnosis, performance prediction of solar air collectors). The best-performing models featured a number of rewirings consistent with the small-world regime. However, all assessed topologies were constrained by MLP-random interpolation. In [2], an MLP and a NN generated following the Barabási-Albert (BA) procedure were compared on a chemical process modeling problem. Both models were trained with an evolutionary algorithm, but the MLP achieved a lower RMSE. The *learning matrix* [24], a sequential algorithm for the forward/backward pass of arbitrary directed acyclic graphs (DAGs), enabled the evaluation of several well-known complex networks on classification [24] and regression [26] tasks. The experiments included random and small-world networks, two topologies based on “preferential attachment”, a complete graph, and a *C. elegans* sub-network [7]. Nevertheless, the learning matrix’s time complexity limited the network sizes (i.e., 26 nodes), and for each task, a different winning topology emerged, including the MLP. Some recent works have instead focused on mul-

tipartite sparse graphs [23, 35]. While these architectures outperformed the complete baselines, their topological complexity was entirely encoded within the connections between adjacent layers.

We propose the hypothesis that, given the same number of nodes (i.e., neurons) and edges (i.e., parameters), a complex NN might exhibit superior predictive abilities compared to classical, more regularly structured MLPs. Unlike previous studies, we conduct a systematic exploration of random, scale-free, and small-world graphs (Figure 1) on synthetic classification tasks, with particular emphasis on the following:

- **Network size.** The defining properties of a complex topology often emerge in large-scale networks. For example, the second moment of a power-law degree distribution diverges only in the $N \rightarrow \infty$ limit [3], where N is the network size¹. The networks in [24, 26] have 15 and 26 nodes, respectively. We trained models with 128 neurons.
- **Dataset size.** The *estimation error* achieved by a predictor depends on the training set size: the greater the number of samples, the lower the error [30]. Except for studies based on multipartite graphs, all previous research works in a small-data regime. Our datasets are three times larger than those used before.
- **Hyperparameter optimization.** Learning rate and batch size are crucial in minimizing the loss function. Ref. [24] is the only one that considers finding the optimal learning rate. The role of batch size has never been investigated. Each DAG, however, could be characterized by its optimal combination of hyperparameters. Hence, we optimized the learning rate and batch size for each topology.

2 Theory

Complex Graph Generators

Erdős-Rényi (ER). An ER graph [8], or *random network*, is uniformly sampled from the set of all graphs with N nodes and L edges. For $N \gg \langle k \rangle$, the degree distribution of a random graph is well approximated by a Poisson distribution: $p_k = e^{-\langle k \rangle} \frac{\langle k \rangle^k}{k!}$; k and $\langle k \rangle$ represent node degree and average degree, respectively.

Watts-Strogatz (WS). The WS generator [34] aims to create graphs that exhibit both high clustering and the *small-world* property; this is achieved by interpolating *lattices* with random networks. The generation starts from a ring in which nodes are connected to their immediate neighbors. The links are then randomly rewired with probability p .

Barabási-Albert (BA). The well-known BA model [1] can be used to generate networks characterized by the $p_k \propto k^{-3}$ *scale-free* degree distribution. Being

¹The proposition holds when the degree exponent is smaller than 3.

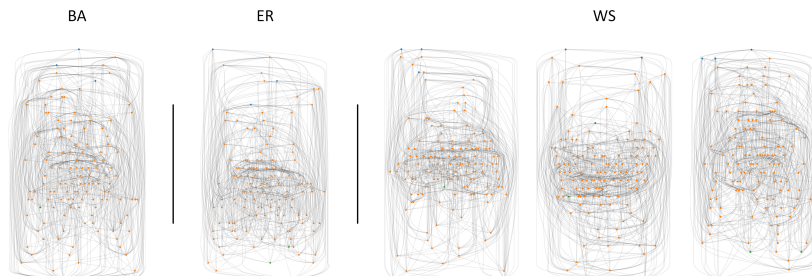


Figure 1: Example feedforward NNs (128 neurons, 732 synaptic connections) based on complex topologies: scale-free (BA), random (ER), and small-world (WS). All graphs are directed and acyclic. Information flows from top to bottom. Input, hidden, and output units are denoted in blue, orange, and green, respectively. Since the networks are defined at the micro-scale, hidden and output nodes implement weighted sums over the incoming edges. In the hidden units, the computational operation is followed by an activation function. The activations of nodes located on the same horizontal layer can be computed in parallel.

the model inspired by the growth of real networks, the generative procedure iteratively attaches nodes with m stubs to a graph that evolves from an initial star of $m + 1$ nodes. Node additions respond to the preferential attachment mechanism: the probability that a stub reaches a node is proportional to the degree of the latter.

Multilayer Perceptron (MLP). The underlying networks of MLPs are called multipartite graphs. In a multipartite graph (i.e., a sequence of bipartite graphs) nodes are partitioned into layers, and each layer can only be connected with the adjacent ones; no intra-layer link is allowed. Additionally, inter-layer connections have to form *bicliques* (i.e., fully-connected bipartite graphs).

3 Methods

3.1 Datasets

The foundation of the datasets developed, as displayed in Figure 2, is established by manifold learning generators² provided by the `scikit-learn` machine learning library [25]. To modify the generators for classification purposes, 3D points sampled from one of the available curves (*s curve* and *swiss roll*) are segmented into `n_classes` \times `n_reps` portions based on their univariate position relative to the primary dimension of the manifold samples. As the term implies, `n_classes` refers to the number of classes involved in the considered classification. Each segment is then arbitrarily allocated to a class, maintaining task balance (i.e.,

²https://scikit-learn.org/stable/datasets/sample_generators.html

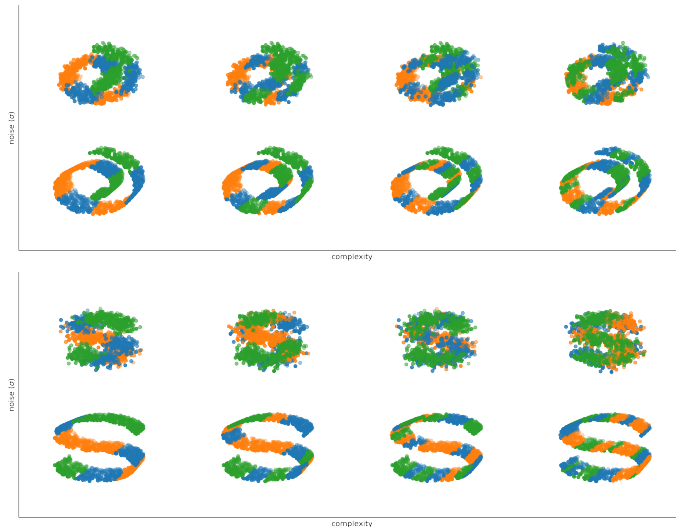


Figure 2: Benchmark classification datasets. **Top:** the *swiss roll*. **Bottom:** the *s curve*. Each dataset is composed of 3D points divided into multiple segments. Classes are color-coded. Datasets differ in terms of difficulty (x axis) and noise (y axis).

precisely `n_reps` segments have the same label). We define `n_reps` as the task *difficulty*. An additional aspect of our datasets is the standard deviation σ of the Gaussian noise that can be added to the points. The generation procedure is finalized with a min-max normalization.

3.2 Feedforward Neural Networks

All trainable models are produced following the same 3-step procedure and share N and L . Consequently, NNs exhibit identical density and parameter counts.

Undirected Graph Generation. The initial step in creating a NN involves sampling an undirected graph using the generators detailed in Section 2. Once N and L are established, all models exhibit a single parameter configuration compatible with the required density³. The WS generator is the sole exception: the probability p is allowed to vary between 0 and 1. If the generator is limited to sample networks with a number of links from a finite set (e.g., $L = m + (N - m - 1)m$ according to the BA model), we first generate a graph with slightly higher density than the target before randomly eliminating excess edges. After obtaining the graph, we confirm the existence of a single connected component.

Directed Acyclic Graph (DAG) Conversion. Before performing any calculations, the direction for information propagation through the network links

³This statement is accurate if the number of MLP layers is predetermined.

must be determined; this is accomplished by randomly assigning, without replacement, an integer index from $\{1, \dots, N\}$ to the network nodes. It can be shown that the directed graph obtained by setting the direction of each edge from the node with a lower index to the node with a higher index is free of cycles. However, this conversion results in an unpredictable number of sources and sinks. Since classification tasks typically involve a pre-defined number of input features and output classes, it is necessary to resolve such network-task discrepancies. To address this issue, we developed a straightforward heuristic capable of adjusting DAGs without altering the underlying undirected graphs.

Mapping of Functional Roles. The last step of the presented procedure consists in mapping computational operations to the DAG nodes. Working at the micro-scale (i.e., connections between single neurons), the operations allowed are two. Source nodes implement constant functions; their role, indeed, is to feed the network with the initial conditions for computations. Hidden and sink nodes, instead, perform a weighted sum over the incoming edges, followed by an activation function:

$$a_v = \sigma \left(\sum_u w_{uv} a_u + b \right) \quad (1)$$

where a_v is the activation of node v , σ denotes the activation function⁴ (SELU [20] for hidden nodes and the identity function for sinks), u represents the generic predecessor of v , w_{uv} is the weight associated with edge (u, v) and b the bias. In order to implement the map of functional roles, we made use of the 4Ward library⁵ [6], developed for the purpose. Starting from a DAG, the package returns a working NN deployable as a PyTorch `Module`.

3.3 Experiments

Dataset Partitioning. Each generated dataset is randomly divided into 3 non-overlapping subsets: the train, validation and test splits. All model trainings are performed over the train split while the validation split is exploited in validation epochs and hyperparameter optimization. Test samples, instead, are accessed only in the evaluation of the final models.

Model Training. Models are trained by minimizing cross entropy with the Adam [19] optimizer ($\beta_1 = 0.9$, $\beta_2 = 0.999$). A scheduler reduces the learning rate by a factor of 0.5 if no improvement is seen on the validation loss for 10 epochs. The training procedure ends when learning stagnates (w.r.t. the validation loss) for 15 epochs, and the model weights corresponding to the epoch in which the minimum validation loss has been achieved are saved.

Hyperparameter Optimization. Hyperparameters are optimized through a grid search over a predefined 2D space (i.e., learning rate/batch size). We generate networks of the same topological family starting from 5 different random seeds.

⁴Depending on the context, we use the same σ notation for both the standard deviation of the dataset noise and the activation function.

⁵<https://github.com/BoCtrl-C/forward>

In the MLP case, models differ only in the weight initialization. For each parameter pair, the 5 models are trained accordingly, and the resulting best validation losses are collected. Then, the learning rate and batch size that minimize the median validation loss computed across the generation seeds are selected as the optimal hyperparameters of the considered graph family.

Topology Evaluation. Once the optimal learning rate and batch size are found, we train 15 new models characterized by the considered topology and compute mean classification accuracy and standard deviation on the dataset test split. The procedure is repeated for each investigated graph family and a Kruskal-Wallis (H-test) [21] is performed in order to test the null hypothesis that the medians of all accuracy populations are equal. If the null hypothesis is rejected, a Mann-Whitney (U-test) [22] post hoc analysis follows.

Robustness Analysis. We use the final trained models in a *graph damage* study to investigate their *functional* robustness (accuracy vs. fraction of removed nodes). The *topological* robustness (giant component vs. fraction of removed nodes) is already well-studied in network science. We randomly remove a fixed fraction of nodes, f , from a neural network and compute the accuracy achieved by the resulting model on the test dataset. Practically, node removal is implemented using PyTorch’s `Dropout`⁶, which zeroes some network activations by sampling from i.i.d. Bernoulli distributions. As each batch element is associated with specific random variables, activations produced by different dataset samples are processed by differently pruned neural networks. Therefore, the figure of interest is averaged over the dataset and the 15 generation seeds. In a typical topological analysis, when $f = 0$, the giant components of all tested graphs have the same size (i.e., N). We adopt this convention in our experimental setup by replacing test accuracy with *accuracy gain*: $\mathcal{A}(f)$. The metric is defined as the ratio between the accuracy obtained by a pruned network and the accuracy obtained by the original one (i.e., $f = 0$). An accuracy gain < 1 indicates a decline in model performance. Consequently, the figure of merit for our analysis is the mean accuracy gain, with the expectation taken over the generation seeds.

4 Results

We obtained the presented results by following the experimental protocol outlined in Section 3 using the specified topologies (i.e., BA, ER, MLP, and WS) and datasets. We set `n_classes = 3` and `n_reps` \in `3, 6, 9, 12`; for the *swiss roll* dataset, $\sigma \in 0.0, 1.0$, while for the *s curve*, $\sigma \in 0.0, 0.3$. The train, validation, and test split sizes were 1350, 675, and 675, respectively. Given that in a 1-hidden layer MLP (`h1` notation) the number of synaptic connections depends solely on N (i.e., $L = 3 \times H + H \times 3$, with $H = N - 3 - 3$), we chose an MLP with 128 neurons as a reference model and calculated the hyperparameters for the complex networks to achieve graphs with $L = 732$ edges. The additional

⁶<https://pytorch.org/docs/stable/generated/torch.nn.Dropout.html>

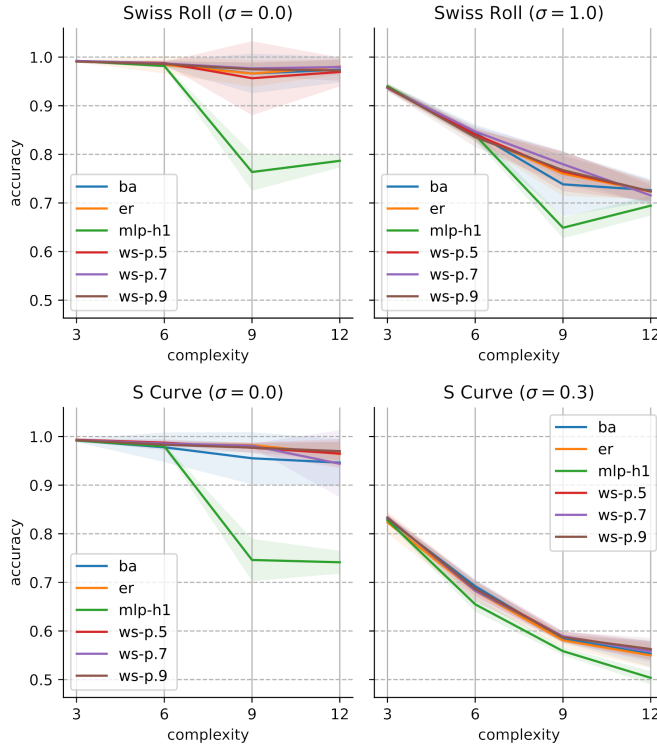


Figure 3: Mean test accuracy as a function of the task difficulty. Confidence intervals (\pm standard deviation) are reported as well. Different subplots correspond to different datasets. Each curve denotes the trend of a specific network topology.

degree of freedom in the WS generator enabled us to separate the small-world topology into three distinct graph families: p.5 ($p = 0.5$), p.7 ($p = 0.7$), and p.9 ($p = 0.9$). The hyperparameter optimization searched for learning rates in $\{0.03, 0.01, 0.003, 0.001\}$ and batch sizes in $\{32, 64\}$.

Figure 3 displays the mean test accuracy achieved by each group of models as a function of task difficulty. All manifolds, noise levels, and difficulties are represented. Excluding difficulty level 9 in the *swiss roll* dataset, the accuracy curves exhibit a clear decreasing trend. Specifically, as the difficulty increases, the performance of the MLPs degrades more rapidly than that of complex networks. Confidence intervals, on the other hand, are wider in the high-difficulty plot regions. As expected, noisy tasks were more challenging to learn.

In Figure 4, the results obtained by the models for the two highest levels of task difficulty are shown in detail. The H-test null hypothesis is rejected for all experiments, and the U-test statistical annotations are displayed. Regardless of the scenario considered, a complex topology consistently holds the top spot in

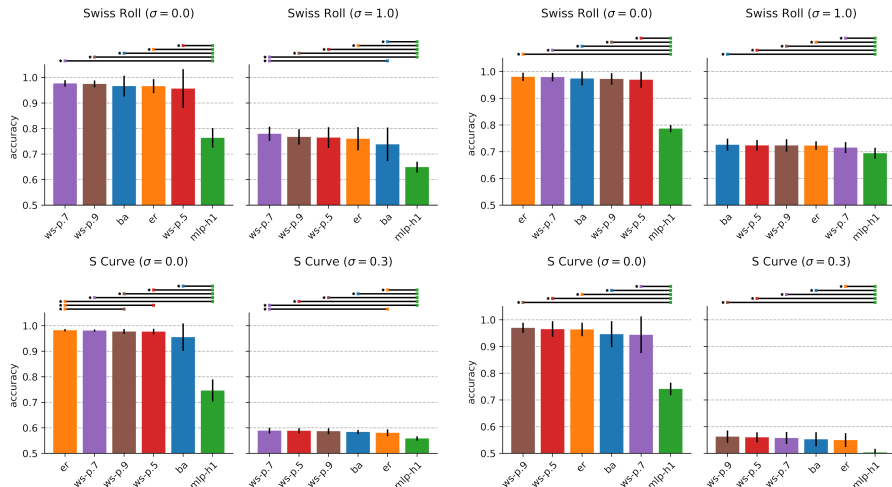


Figure 4: Mean test accuracy at the highest difficulty levels. **Left:** difficulty = 9. **Right:** difficulty = 12. The bars display both means and standard deviations. Each bar corresponds to a specific network topology and is represented by a consistent color across all histograms (following the color scheme from Figure 3). Statistical annotations appear above the histograms, with each segment indicating a significant difference between two accuracy distributions.

the mean accuracy ranking. MLPs, in contrast, are always the worst-performing models. Moreover, the MLP performance differs significantly from that of the complex networks, in a statistical sense. Conversely, only 3 out of 8 experiments exhibit statistical differences within the group of complex networks.

Figure 5 presents the results of the robustness analysis. We investigated $f \in \{0.0, 0.1, \dots, 0.5\}$ and removed nodes from the models trained on the datasets characterized by the lowest level of difficulty. On these tasks, indeed, all models behave approximately the same (see Figure 3), hinting at a fair comparison. Unsurprisingly, node removal has the same effect on all topologies: the accuracy gain decreases as f increases. MLPs, however, show enhanced robustness to random deletions. Confidence intervals of the complex graph families overlap. It is worth noting that the chance level (i.e., accuracy of $1/3$) could be reached by different accuracy gains depending on the task; the best accuracy under $f = 0$, indeed, varies between the manifold/noise pairs.

5 Discussion

The most significant finding from the experiments performed is the performance in terms of accuracy attained by the architectures built on complex topologies in the high-difficulty regime. In this context, and in light of the statistical tests

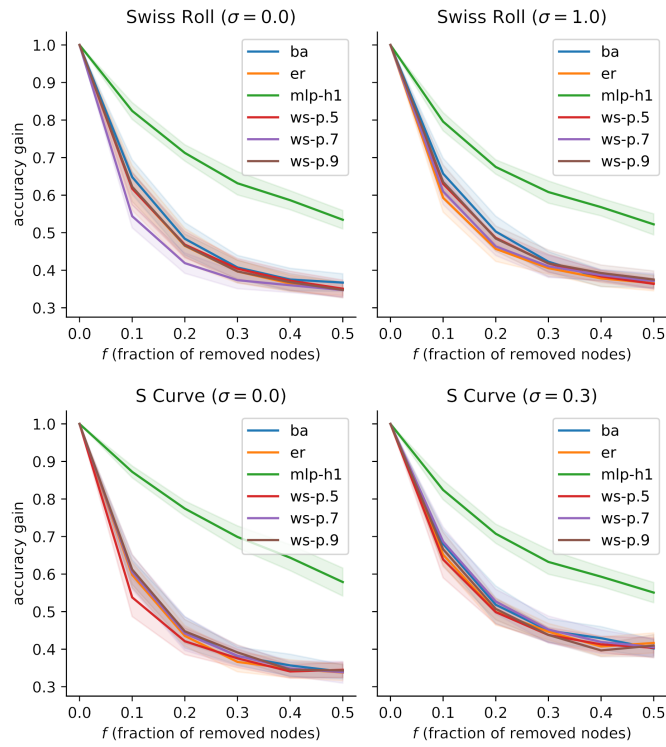


Figure 5: Robustness analysis. The horizontal axis reports the fraction of removed nodes (i.e., f) while the vertical one the accuracy gain (i.e., $\mathcal{A}(f)$). Each curve refers to a different network topology. Confidence intervals (\pm standard deviation) are reported.

carried out, the complex models prove to be a solid alternative to MLPs.

Formally justifying the observed phenomenon is challenging. Fortunately, in 2017, Poggio et al. discussed two theorems [28] that guided our explanation. According to the first theorem⁷, a shallow network (e.g., an MLP **h1**) equipped with infinitely differentiable activation functions requires $N = \mathcal{O}(\epsilon^{-n})$ units to approximate a continuous function f of n variables⁸ with an approximation error of at most $\epsilon > 0$. This exponential dependency is technically called the *curse of dimensionality*. On the other hand, the second theorem states that if f is compositional and the network presents its same architecture, we can escape the “curse”. It is important to remember that a compositional function is defined as a composition of “local” constituent functions, $h \in \mathcal{H}$ (e.g., $f(x_1, x_2, x_3) = h_2(h_1(x_1, x_2), x_3)$, where x_1, x_2, x_3 are the input variables and h_1, h_2 the constituent functions). In other words, the structure of a compositional function can be represented by a DAG. In this approximation scenario, the required number of units depends on $N = \mathcal{O}(\sum_h \epsilon^{-n_h})$, where n_h is the input dimensionality of function h . If $\max_h n_h = d$, then $\sum_h \epsilon^{-n_h} \leq \sum_h \epsilon^{-d} = |\mathcal{H}| \epsilon^{-d}$.

The primary advantage of complex networks is their potential to avoid the curse of dimensionality when relevant graphs for the function to be learned are present. Under the assumption that the function linking the *swiss roll* and *s curve* points to the ground truth labels is compositional (intuitively, in non-noisy datasets, each class is a union of various segments), we conjecture that our complex NNs can exploit this compositionality. In the high-difficulty regime, the necessary network size for MLP **h1** to achieve the same accuracy as complex models likely exceeds the size set for experiments. While one could argue that the datasets employed were compositionally sparse by chance, according to [27], all *efficiently computable functions* must be *compositionally sparse* (i.e., their constituent functions have “small” d). Performance differences on noisy datasets are less noticeable, possibly due to the minimal overlap between the functions to be approximated and the studied topologies. Notably, our setup does not precisely match the theorem formulations in [28] (e.g., SELUs are not infinitely differentiable), but Poggio et al. argue that the hypotheses can likely be relaxed. No statistically significant differences emerged between the complex graph families from the results of Section 4. Various explanations exist for this outcome: all tested topologies could be complex enough to include relevant subgraphs of the target f functions; the random DAG conversion heuristic might have perturbed hidden topological properties of the original undirected networks; or the degree distribution of a network may not be the most relevant topological feature in a model’s approximation capabilities.

However, the higher accuracy in complex networks comes with trade-offs. Although the methodology in [6] improves the scalability of complex NNs and enables experimentation with arbitrary DAGs, it is important to note that 1-hidden layer MLPs typically have faster forward pass computation. In these models, the forward pass requires only two matrix multiplications, whereas, in

⁷We invite the reader to consult ref. [28] for a complete formulation of the theorems.

⁸Depending on the context, we use the same f notation for both the fraction of removed nodes and the function to be approximated.

NNs built using 4Ward, the number of operations depends on the DAG *height*. Moreover, the analyses in Figure 5 demonstrate MLPs’ superiority in a graph damage scenario. We speculate that the hidden units in an MLP **h1** contribute equally to the approximation of the target function. In contrast, the ability of complex networks to exploit the compositionality of the function to be learned might lead to high specialization of some hidden units.

6 Conclusion

Our study provides valuable insights into the influence of network topology on the approximation capabilities of artificial neural networks (ANNs). Our novel methodology for constructing complex ANNs based on various topologies has enabled a systematic exploration of the impact of network structure on model performance. The experiments conducted on synthetic datasets demonstrate the potential advantages of complex topologies in high-difficulty regimes when compared to traditional MLPs.

While complex networks exhibit improved performance, this comes at the cost of increased computational requirements and reduced robustness to graph damage. Our investigation of the relationship between topological attributes and model performance (Appendix A) reveals a complex interplay that cannot be explained by any single attribute. This finding highlights the need for further research to better understand the interactions among multiple topological attributes and their impact on ANN performance.

As a result of this study, researchers and practitioners can consider the potential benefits and limitations of complex topologies when designing ANNs for various tasks. Moreover, our work provides a foundation for future research focused on identifying optimal topological features, understanding the impact of multiple attributes, and developing new methodologies for constructing more efficient and robust ANN architectures. By further exploring the role of network topology in ANNs, we can unlock new possibilities for improving the performance and adaptability of these models across diverse applications.

References

- [1] Réka Albert and Albert-László Barabási. Statistical mechanics of complex networks. *Reviews of modern physics*, 74(1):47, 2002.
- [2] Mauro Annunziato, Ilaria Bertini, Matteo De Felice, and Stefano Pizzuti. Evolving Complex Neural Networks. In Roberto Basili and Maria Teresa Pazienza, editors, *AI*IA 2007: Artificial Intelligence and Human-Oriented Computing*, volume 4733, pages 194–205. Springer Berlin Heidelberg, Berlin, Heidelberg, 2007. Series Title: Lecture Notes in Computer Science.
- [3] A.L. Barabási. *Network Science*. Cambridge University Press, 2016.

- [4] Marc Barthelemy. Betweenness centrality in large complex networks. *The European physical journal B*, 38(2):163–168, 2004.
- [5] Danielle S Bassett, Daniel L Greenfield, Andreas Meyer-Lindenberg, Daniel R Weinberger, Simon W Moore, and Edward T Bullmore. Efficient physical embedding of topologically complex information processing networks in brains and computer circuits. *PLoS computational biology*, 6(4):e1000748, 2010.
- [6] Tommaso Boccatto, Matteo Ferrante, Andrea Duggento, and Nicola Toschi. 4ward: a relayering strategy for efficient training of arbitrarily complex directed acyclic graphs, 2022.
- [7] Nathan A. Dunn, Shawn R. Lockery, Jonathan T. Pierce-Shimomura, and John S. Conery. A neural network model of chemotaxis predicts functions of synaptic connections in the nematode *Caenorhabditis elegans*. *J. Comput. Neurosci.*, 17(2):137–147, 2004.
- [8] Paul Erdős, Alfréd Rényi, et al. On the evolution of random graphs. *Publ. Math. Inst. Hung. Acad. Sci.*, 5(1):17–60, 1960.
- [9] Okan ErKaymaz and Mahmut Ozer. Impact of small-world network topology on the conventional artificial neural network for the diagnosis of diabetes. *Chaos, Solitons & Fractals*, 83:178–185, February 2016.
- [10] Okan ErKaymaz, Mahmut Ozer, and Matjaž Perc. Performance of small-world feedforward neural networks for the diagnosis of diabetes. *Applied Mathematics and Computation*, 311:22–28, October 2017.
- [11] Okan ErKaymaz, Mahmut Özer, and Nejat Yumuşak. Impact of small-world topology on the performance of a feed-forward artificial neural network based on 2 different real-life problems. page 12.
- [12] Okan ErKaymaz, Mahmut Özer, and Nejat Yumuşak. Performance Analysis of A Feed-Forward Artifical Neural Network With Small-World Topology. *Procedia Technology*, 1:291–296, 2012.
- [13] Frederic B. Fitch. Warren s. mcculloch and walter pitts. a logical calculus of the ideas immanent in nervous activity. bulletin of mathematical biophysics, vol. 5 (1943), pp. 115–133. *Journal of Symbolic Logic*, 9(2):49–50, 1944.
- [14] Alex Fornito, Andrew Zalesky, and Michael Breakspear. Graph analysis of the human connectome: Promise, progress, and pitfalls. *NeuroImage*, 80:426–444, 2013. Mapping the Connectome.
- [15] Aric A. Hagberg, Daniel A. Schult, and Pieter J. Swart. Exploring network structure, dynamics, and function using networkx. In Gaël Varoquaux, Travis Vaught, and Jarrod Millman, editors, *Proceedings of the 7th Python in Science Conference*, pages 11 – 15, Pasadena, CA USA, 2008.

- [16] Kaiming He, Xiangyu Zhang, Shaoqing Ren, and Jian Sun. Deep residual learning for image recognition. In *2016 IEEE Conference on Computer Vision and Pattern Recognition (CVPR)*, pages 770–778, 2016.
- [17] Gao Huang, Zhuang Liu, Laurens Van Der Maaten, and Kilian Q. Weinberger. Densely connected convolutional networks. In *2017 IEEE Conference on Computer Vision and Pattern Recognition (CVPR)*, pages 2261–2269, 2017.
- [18] Sara Kaviani and Insoo Sohn. Application of complex systems topologies in artificial neural networks optimization: An overview. *Expert Systems with Applications*, 180:115073, 2021.
- [19] Diederik P. Kingma and Jimmy Ba. Adam: A method for stochastic optimization. In Yoshua Bengio and Yann LeCun, editors, *3rd International Conference on Learning Representations, ICLR 2015, San Diego, CA, USA, May 7-9, 2015, Conference Track Proceedings*, 2015.
- [20] Günter Klambauer, Thomas Unterthiner, Andreas Mayr, and Sepp Hochreiter. Self-normalizing neural networks. In I. Guyon, U. Von Luxburg, S. Bengio, H. Wallach, R. Fergus, S. Vishwanathan, and R. Garnett, editors, *Advances in Neural Information Processing Systems*, volume 30. Curran Associates, Inc., 2017.
- [21] William H. Kruskal and W. Allen Wallis. Use of ranks in one-criterion variance analysis. *Journal of the American Statistical Association*, 47(260):583–621, 1952.
- [22] H. B. Mann and D. R. Whitney. On a test of whether one of two random variables is stochastically larger than the other. *The Annals of Mathematical Statistics*, 18(1):50–60, 1947.
- [23] Decebal Constantin Mocanu, Elena Mocanu, Peter Stone, Phuong H. Nguyen, Madeleine Gibescu, and Antonio Liotta. Scalable training of artificial neural networks with adaptive sparse connectivity inspired by network science. *Nature Communications*, 9(1):2383, December 2018.
- [24] Roberto L. S. Monteiro, Tereza Kelly G. Carneiro, José Roberto A. Fontoura, Valéria L. da Silva, Marcelo A. Moret, and Hernane Borges de Barros Pereira. A Model for Improving the Learning Curves of Artificial Neural Networks. *PLOS ONE*, 11(2):e0149874, February 2016.
- [25] F. Pedregosa, G. Varoquaux, A. Gramfort, V. Michel, B. Thirion, O. Grisel, M. Blondel, P. Prettenhofer, R. Weiss, V. Dubourg, J. Vanderplas, A. Passos, D. Cournapeau, M. Brucher, M. Perrot, and E. Duchesnay. Scikit-learn: Machine learning in Python. *Journal of Machine Learning Research*, 12:2825–2830, 2011.

- [26] Gustavo Mendes Platt, Xin-She Yang, and Antônio José Silva Neto, editors. *Computational Intelligence, Optimization and Inverse Problems with Applications in Engineering*. Springer International Publishing, Cham, 2019.
- [27] Tomaso Poggio. It is Compositional Sparsity: a framework for ML. page 9.
- [28] Tomaso Poggio, Hrushikesh Mhaskar, Lorenzo Rosasco, Brando Miranda, and Qianli Liao. Why and when can deep-but not shallow-networks avoid the curse of dimensionality: A review. *International Journal of Automation and Computing*, pages 1–17, 03/2017 2017.
- [29] Louis K Scheffer, C Shan Xu, Michal Januszewski, Zhiyuan Lu, Shin-ya Takemura, Kenneth J Hayworth, Gary B Huang, Kazunori Shinomiya, Jeremy Maitlin-Shepard, Stuart Berg, Jody Clements, Philip M Hubbard, William T Katz, Lowell Umayam, Ting Zhao, David Ackerman, Tim Blakely, John Bogovic, Tom Dolafi, Dagmar Kainmueller, Takashi Kawase, Khaled A Khairy, Laramie Leavitt, Peter H Li, Larry Lindsey, Nicole Neubarth, Donald J Olbris, Hideo Otsuna, Eric T Trautman, Masayoshi Ito, Alexander S Bates, Jens Goldammer, Tanya Wolff, Robert Svirskas, Philipp Schlegel, Erika Neace, Christopher J Knecht, Chelsea X Alvarado, Dennis A Bailey, Samantha Ballinger, Jolanta A Borycz, Brandon S Canino, Natasha Cheatham, Michael Cook, Marisa Dreher, Octave Duclos, Bryon Eubanks, Kelli Fairbanks, Samantha Finley, Nora Forknall, Audrey Francis, Gary Patrick Hopkins, Emily M Joyce, SungJin Kim, Nicole A Kirk, Julie Kovalyak, Shirley A Lauchie, Alanna Lohff, Charli Maldonado, Emily A Manley, Sari McLin, Caroline Mooney, Miatta Ndama, Omotara Ogundeyi, Nneoma Okeoma, Christopher Ordish, Nicholas Padilla, Christopher M Patrick, Tyler Paterson, Elliott E Phillips, Emily M Phillips, Neha Rampally, Caitlin Ribeiro, Madelaine K Robertson, Jon Thomson Rymer, Sean M Ryan, Megan Sammons, Anne K Scott, Ashley L Scott, Aya Shinomiya, Claire Smith, Kelsey Smith, Natalie L Smith, Margaret A Sobeski, Alia Suleiman, Jackie Swift, Satoko Takemura, Iris Talebi, Dorota Tarnogorska, Emily Tenshaw, Temour Tokhi, John J Walsh, Tansy Yang, Jane Anne Horne, Feng Li, Ruchi Parekh, Patricia K Rivlin, Vivek Jayaraman, Marta Costa, Gregory SXE Jefferis, Kei Ito, Stephan Saalfeld, Reed George, Ian A Meinertzhagen, Gerald M Rubin, Harald F Hess, Viren Jain, and Stephen M Plaza. A connectome and analysis of the adult *Drosophila* central brain. *eLife*, 9:e57443, September 2020.
- [30] Shai Shalev-Shwartz and Shai Ben-David. *Understanding Machine Learning: From Theory to Algorithms*. Cambridge University Press, 2014.
- [31] D. Simard, L. Nadeau, and H. Kröger. Fastest learning in small-world neural networks. *Physics Letters A*, 336(1):8–15, February 2005.
- [32] Karen Simonyan and Andrew Zisserman. Very Deep Convolutional Networks for Large-Scale Image Recognition. *arXiv e-prints*, page arXiv:1409.1556, September 2014.

- [33] Emma K Towilson, Petra E Vértés, Sebastian E Ahnert, William R Schafer, and Edward T Bullmore. The rich club of the *c. elegans* neuronal connectome. *Journal of Neuroscience*, 33(15):6380–6387, 2013.
- [34] Duncan J Watts and Steven H Strogatz. Collective dynamics of ‘small-world’ networks. *nature*, 393(6684):440–442, 1998.
- [35] Jiaxuan You, Jure Leskovec, Kaiming He, and Saining Xie. Graph Structure of Neural Networks. *arXiv:2007.06559 [cs, stat]*, August 2020. arXiv:2007.06559.

A Graph Attributes

We delved deeper into the role of network topology in the models’ approximation capabilities by calculating a total of 27 topological graph attributes for each trained neural network. Our aim was to ascertain if any specific attributes could account for the models’ performance. The correlation plots that display the relationship between test accuracy and graph attribute can be found in Figures 6 and 7.

To compute these metrics, we employed the NetworkX library [15] when feasible, and devised custom implementations for the remaining attributes. We conducted the experiments using noise-free datasets with the highest difficulty levels.

After analyzing the experimental data, no evident relationship emerged between the attributes and the models’ performance. In other words, when examined individually, none of the attributes could account for the achieved accuracies. This outcome implies that the impact of network topology on the approximation capabilities of the models might be more intricate than a straightforward correlation with any single topological attribute. Further investigation is necessary to explore the potential interplay among multiple attributes and their influence on the models’ performance.

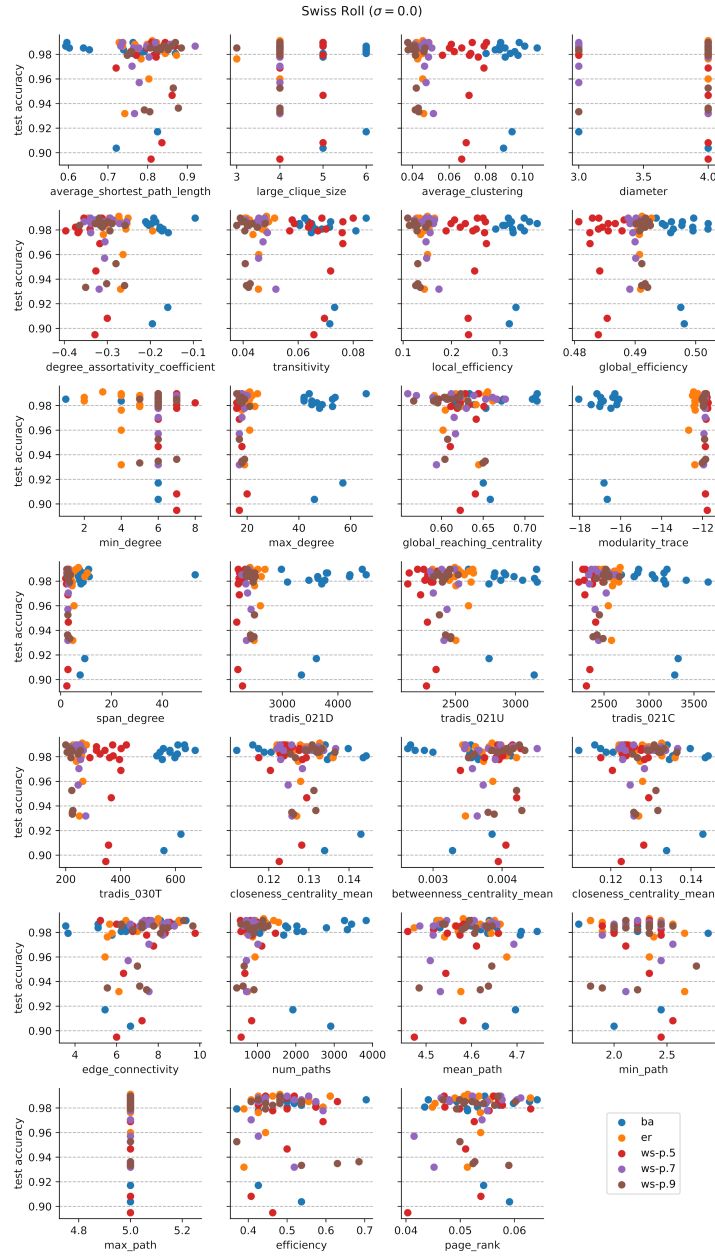


Figure 6: Correlation plots (accuracy vs. attribute) computed on the *swiss roll* dataset ($n_{\text{reps}} = 12$, $\sigma = 0.0$). Each network topology is denoted with a different color, which can be found in the legend (last subplot).

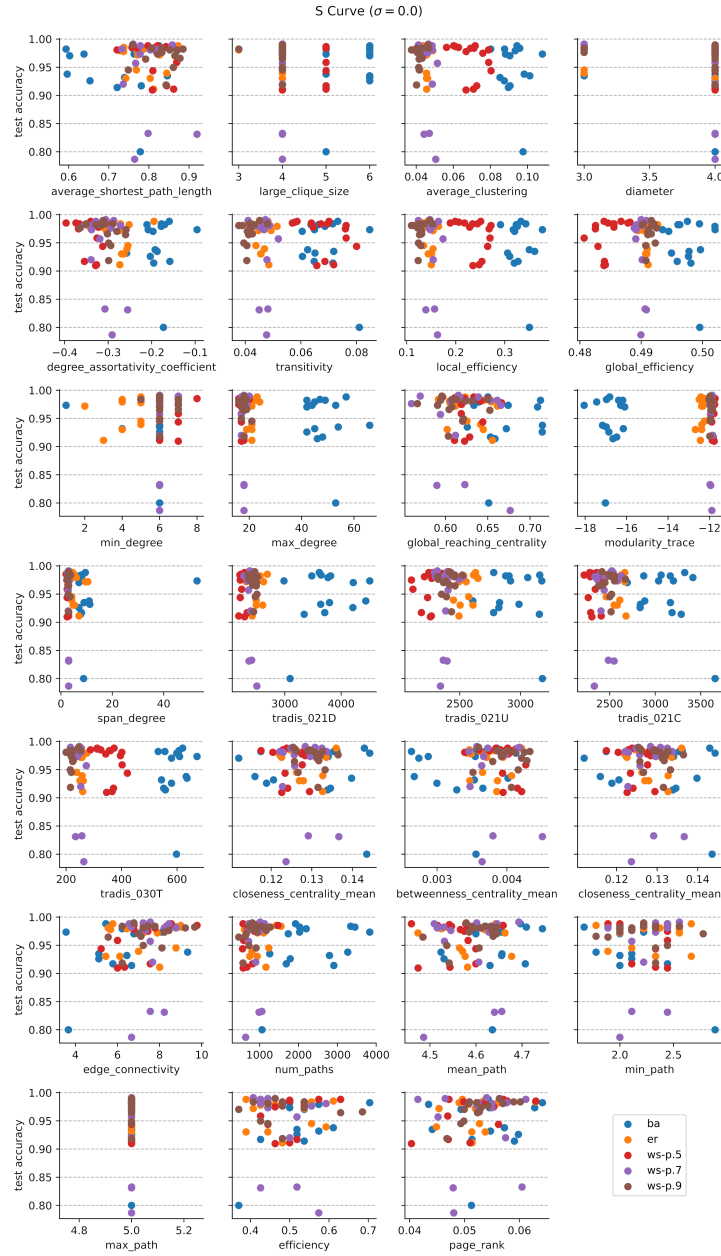


Figure 7: Correlation plots (accuracy vs. attribute) computed on the *s curve* dataset ($n_{\text{reps}} = 12$, $\sigma = 0.0$). Each network topology is denoted with a different color, which can be found in the legend (last subplot).